Available online at www.sciencedirect.com
ScienceDirect
Trans. Nonferrous Met. Soc. China 28(2018) 1714−1723
Transactions of Nonferrous Metals Society of China
www.tnmsc.cn

Effect of Fe content on microstructures and properties of Ti6Al4V alloy with combinatorial approach

Di WU[1], Li-gang ZHANG[1,2], Li-bin LIU[1,3], Wei-min BAI[1], Li-jun ZENG[1]

1. School of Materials Science and Engineering, Central South University, Changsha 410083, China;
2. ZIK Virtuhcon, TU Bergakademie Freiberg, Fuchsmühlenweg 9, D-09596 Freiberg, Germany;
3. Key Laboratory of Non-ferrous Metallic Materials Science and Engineering of Ministry of Education, Central South University, Changsha 410083, China

Received 27 May 2017; accepted 18 December 2017

Abstract: A combinatorial approach was applied to investigating the influence of Fe content on the microstructures and properties of Ti6Al4V alloy. A diffusion couple was manufactured with Ti6Al4V and Ti6Al4V20Fe alloys and annealed at 1000 °C for 600 h to obtain a wide range of compositions. By combining electron probe micro-analysis (EPMA), scanning electron microscopy (SEM) and nanoindentation, the relationships between composition and microstructure as well as hardness were determined. It is found that after aging the Ti6Al4V5Fe sample contains reasonable (about 55%) volume fraction of fine α phase and shows the peak hardness among the Ti6Al4V*x*Fe alloys. Therefore, it is a promising candidate for the development of titanium alloys. HAADF-STEM and XRD reveal that after quenching from the single β phase field, the metastable α'' lamellae form in the Ti6Al4V5Fe alloy, and on subsequent isothermal aging, the α'' lamellae become coarse and act as precursors/preferential nucleation sites for the stable α phase.
Key words: diffusion multiple; Ti6Al4V*x*Fe alloys; composition; microstructure; hardness; HAADF−STEM

1 Introduction

Titanium (Ti) and Ti alloys have a wide variety of applications in aerospace [1], automobiles [2], biomedical [3,4] industries and other areas [5−7]. Amongst titanium alloys, α/β two-phase alloys, e.g., Ti6Al4V, have the widest applications and cover currently more than 50% of the application market share of titanium alloys [1]. This is due to their attractive physical and mechanical properties, such as low density, wide range combination of strength, ductility and toughness as well as excellent corrosion resistance.

Metastable β alloys, including Ti5A15V5Mo3Cr (Ti5553), Ti10V3Al2Fe (Ti1023) and Ti15V3Cr3A13Sn (Ti153), could replace the high-strength aerospace type steels with very high strength levels (1200−1700 MPa) [8−12]. Adding β stabilizing element(s) to the Ti6Al4V alloy may be a promising way of developing new metastable β alloys. In order to do this, a thorough investigation of the influence of the addition of the β stabilizing elements on the microstructure and properties of the Ti6Al4V alloy is indispensable.

It has been known that Fe is an effective eutectoid β stabilizing element [13−15]. From the early commercially significant β alloy Ti10V2Fe3Al (Ti1023) [16], Ti4.5Fe6.8Mo1.5A1 (Ti-LCB) [17], to Ti−6V−6Mo−6Fe−3Al (Ti6663) [18], Fe has been used for many years as a major constituent in high-strength titanium alloys. KANOU et al [19] have investigated the effect of 3%−4% (mass fraction) Fe addition on the mechanical properties of Ti6Al4V alloys produced by the prealloyed powder method; while there is not even enough investigation of the effects of Fe on the microstructures and mechanical properties of Ti6Al4V alloy. In addition, Fe was also often selected for its low cost [20]. It could be a suitable element to modify the Ti6Al4V alloy.

A diffusion-multiple approach was developed recently to efficiently map phase diagrams and study materials properties [21,22]. This approach forms

Foundation item: Project (2014CB644000) supported by the National Basic Research Program of China; Project (2016YFB0701301) supported by the National Key Technology R&D Program of China; Projects (51371200, 51671218) supported by the National Natural Science Foundation of China; Project supported by State Key Laboratory of Powder Metallurgy, Central South University, China
Corresponding author: Li-bin LIU, Li-gang ZHANG; Tel: +86-731-88877732; Fax: +86-731-88876692; E-mail: lbliu@csu.edu.cn, ligangzhang@csu.edu.cn
DOI: 10.1016/S1003-6326(18)64815-0

continuous composition gradients of alloying elements in one sample. Combined with different kinds of micro-probe, we can rapidly analyze different properties in rather large composition space generated by diffusion multiples, which would greatly reduce the time spent for each step of making an ingot of individual composition, homogenizing it, preparing a sample, and loading it into different testing systems. Through this approach, ZHAO [23], WU et al [24] and ZHANG et al [25] have established a database of composition dependent elastic modulus and hardness of the Ti−Zr−Ta systems, which might provide a significant guide for the alloy design of new type bio-titanium alloys. However, a lot of titanium alloys data are also lacking, such as the effect of Fe addition on the microstructure and properties of titanium alloys.

The purpose of this work was to develop a new high-strength alloy in Ti−Al−V−Fe system. In this work, a Ti6Al4V−Ti6Al4V20Fe diffusion couple with continuous composition gradient of Fe was prepared. By combining nano-indentation, scanning electron microscopy (SEM) and electron probe micro-analysis (EPMA), the relationships among composition, microstructure and properties of the diffusion multiple were determined. The morphology and phase transformation of Ti6Al4V5Fe were determined by high-angle annular dark field-scanning transmission electron microscope (HAADF-STEM) and the energy-dispersive spectrometer (EDS) equipped on the FEI Titan 80−300 microscope.

2 Experimental

The alloying elements used are Al (99.99% pure), V (99.95% pure), and Fe (99.95% pure). The Ti6Al4V was supplied by Baosteel and its chemical compositions are listed in Table 1.

Table 1 Chemical compositions of as-received Ti6Al4V and Ti6Al4V20Fe (mass fraction, %)

Alloy	Al	V	Fe	O	N	C	Ti
Ti6Al4V	6.37	3.61	0.13	0.18	0.02	0.02	Bal.
Ti6Al4V20Fe	6.16	3.82	19.54	0.09	0.016	0.011	Bal.

Ti6Al4V20Fe was prepared using a commercial arc-melting vacuum casting system. The ingots were re-melted five times prior to casting to improve their chemical homogeneity. Ti6Al4V and Ti6Al4V20Fe were cut into pieces of 8 mm × 8 mm × 4 mm using electro-discharge machining (EDM). The bonding faces of the diffusion couples were ground and polished to a final finish with 0.25 μm alumina slurry. The polished metal surfaces were ultrasonically cleaned in ethanol and dried in hot air, and then the couples were clamped in steel fixtures with a minimum pressure to ensure good contact and annealed at 1000 °C for 10 h in vacuum (~10^{-7} kPa). The Ta film was put between the diffusion couple and the steel fixture to act as a diffusion barrier. After that, the diffusion couples were sealed into an evacuated silica capsules and annealed at 1000 °C for 600 h to get a wide range of compositions. Subsequently, the diffusion couples were taken out and water quenched to room temperature. The diffusion couples were then heated to 1050 °C (above β transus temperature) for 6 h and quenched to room temperature. It was followed by aging at 600 °C for 6 h and quenched in water to examine the microstructure and mechanical properties. The heat treatment schedule is shown in Fig. 1.

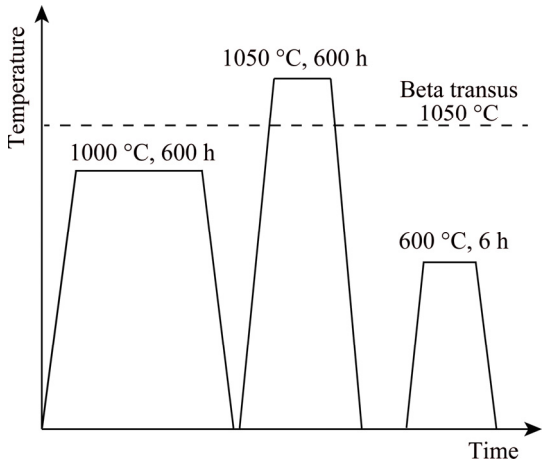

Fig. 1 Heat treatment schedule for Ti6Al4V−Ti6Al4V20Fe diffusion multiple

The diffusion couples were mounted, ground and polished using standard metallographic techniques. The microstructures were investigated using JEOL-JSM 7001F field emission gun-scanning electron microscope (FEG−SEM) operating at voltage of 20 kV and working distance of 10 mm and equipped with an XMax Oxford energy dispersive X-ray spectrometer (EDS). Nano-indentation test was performed at room temperature using a nano indenter UNHT (CSM Instruments, Peseux, Switzerland) with a Berkovich diamond indenter. The applied load was 500 mN with a peak hold time of 15 s. Finally, the composition near indentation was measured by quantitative EPMA analysis on a JEOL JXA−8230 microprobe with 15 kV, 20 nA and 40° take-off angle.

Alloys with optimal compositions were prepared from pure Ti, Fe, Al and V in a commercial arc-melting vacuum casting system. The ingots, of approximately 10 g each, were re-melted five times to improve their chemical homogeneity. The ingots were sealed into evacuated silica capsules at 1050 °C for 6 h, water quenched to room temperature and then aged in the preheated furnace at 600 °C for 6 h. After that, the phase

analysis was conducted using a diffractometer (XRD−6000, Shimadzu, Japan). TEM was performed on a FEI Titan 80−300 microscope at an accelerating voltage of 300 kV. High-angle annular dark field (HAADF) images were acquired with 50 and 180 mrad inner and outer collection angles, respectively. The elemental partitioning between the α phase and the β phase was determined by the energy-dispersive spectrometer (EDS) equipped in the FEI Titan 80−300 microscope.

3 Results

3.1 Continuous composition gradient of Ti6Al4V−Ti6Al4V20Fe system

The variation of composition as a function of distance for the Ti6Al4V−Ti6Al4V20Fe system is plotted in Fig. 2. It could be found that Fe diffuses into Ti6Al4V alloy and mainly substitutes Ti.

3.2 Microstructure of Ti6Al4V*x*Fe alloys after β annealing

Backscatter electron micrographs of Ti6Al4V and the series of Ti6Al4V*x*Fe alloys solution-treated at 1050 °C are shown in Fig. 3. As shown in Figs. 3(a) and (b), the quenched microstructures of Ti6Al4V and Ti6Al4V1Fe alloy contain hexagonal α' martensite phase with coarse lath structures. With the increase of Fe content to 2%−3% (mass fraction), the amount of martensitic laths increases and the size of them decreases, as shown in Figs. 3(c) and (d). When Fe content is increased to 4%, the fine acicular structure of the α' phase and a significant amount of equiaxed retained β phase are observed, and the α' phase presents only at the

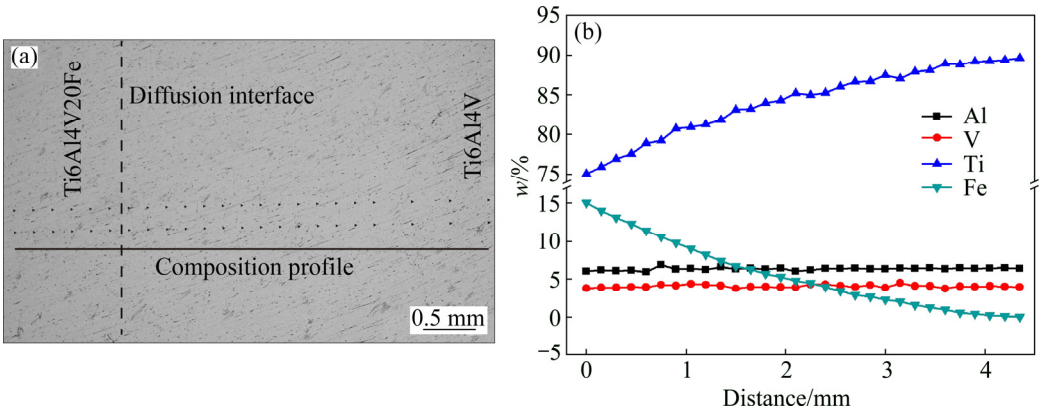

Fig. 2 Optical image of nanoindentation grid (a) and variation in composition as function of distance (b) for Ti6Al4V−Ti6Al4V20Fe diffusion multiple

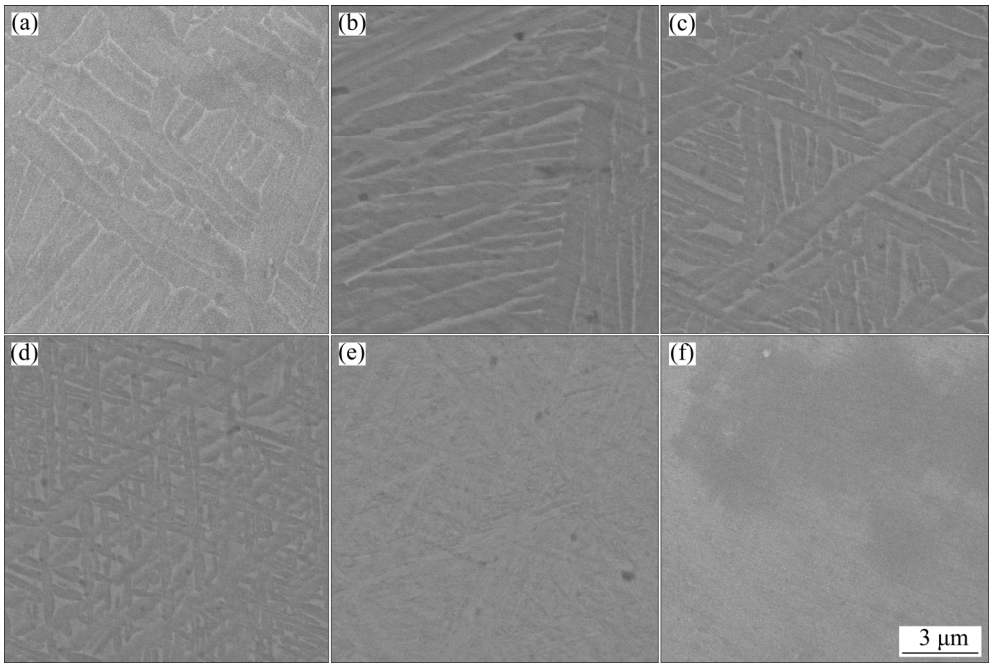

Fig. 3 Backscattered electron SEM images of β-annealed Ti6Al4V*x*Fe alloys with different Fe mass fractions of 0 (a), 1% (b), 2% (c), 3% (d), 4% (e) and 5% (f) taken from Ti6Al4V−Ti6Al4V20Fe diffusion multiple

grain boundary of the β phase, as shown in Fig. 3(e). When the alloy contains 5% or more Fe, almost only β phase can be found (Fig. 3(f)). In other words, the β phase can be entirely retained upon fast cooling, i.e., the martensitic starting temperature (M_s) dropped below room temperature and the β-to-α' martensitic transformation is completely suppressed. However, it should be noted that the ω and α'' phases are too small to be seen by SEM microscopy. Supression of the β-to-α' martensitic transformation does not mean suppression of all the phase transformation. This will be shown in the TEM analysis and is in agreement with previous studies of other Ti alloys [26,27].

3.3 Microstructure of Ti6Al4V*x*Fe alloys after aging

The microstructures of the series of Ti6Al4V*x*Fe alloys are shown in Fig. 4 after aging at 600 °C for 6 h. As shown in Figs. 4(a) and (b), the Ti6Al4V and Ti6Al4V1Fe alloys contain Widmanstätten structure with basket weave morphology. When 2%−3% Fe is added,

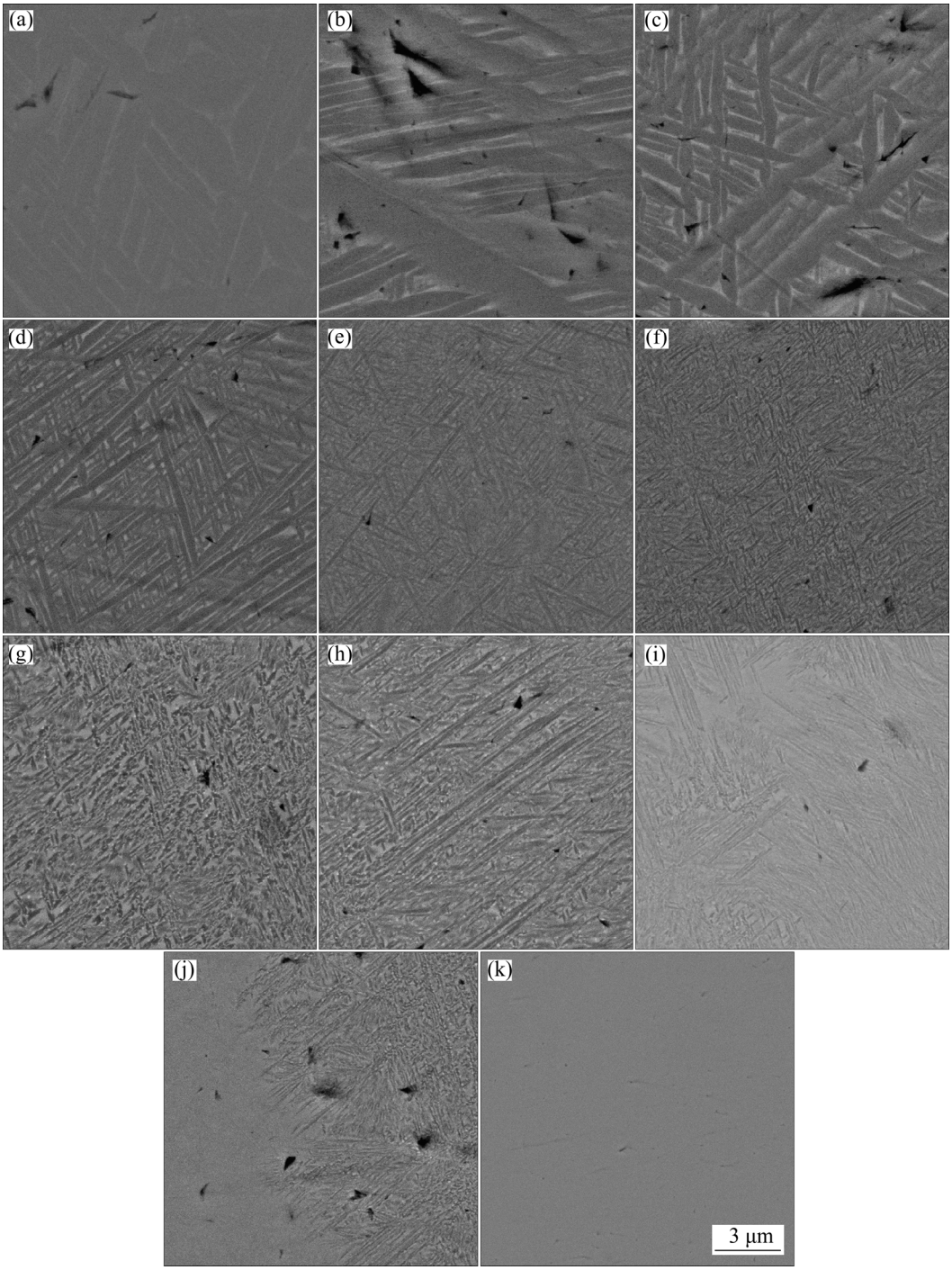

Fig. 4 Backscattered electron SEM images of aged Ti6Al4V*x*Fe alloys with different Fe mass fractions of 0 (a), 1% (b), 2% (c), 3% (d), 4% (e), 5% (f), 7% (g), 9% (h), 11% (i), 13% (j) and 15% (k) taken from Ti6Al4V−Ti6Al4V20Fe diffusion multiple

the microstructure is similar to that of the Ti6Al4V alloy but contains finer α laths, as shown in Figs. 4(c) and (d). When Fe content is 4%, the fine acicular structure of the α phase can be observed, as shown in Fig. 4(e). When the Fe content is increased to 5%, the alloy contains the finest α phase compared with the other alloys, and the nanometer-scale acicular α precipitates are hardly to be observed by SEM. When the Fe content is 7% or higher, the α phases will become coarser, and the volume fraction of intragranular α phase decreases significantly.

3.4 Influence of Fe content on hardness after β annealing and after aging

The variation in Fe content and hardness as a function of the diffusion distance is plotted in Fig. 5. It can be seen that the Fe content has a significant impact on hardness. In the β-annealed condition (Fig. 5(a)), the hardness increases firstly from 4.7 to 5.6 GPa as Fe content increases from 0 to 5% and then rapidly drops to the minimum of 4.4 GPa, when the Fe content increases from 5% to 7%. Finally, the hardness increases again as the Fe content further increases. In the aged condition, the hardness increases firstly from 4.8 to 6.2 GPa as Fe content increases from 0 to 5% and then decreases.

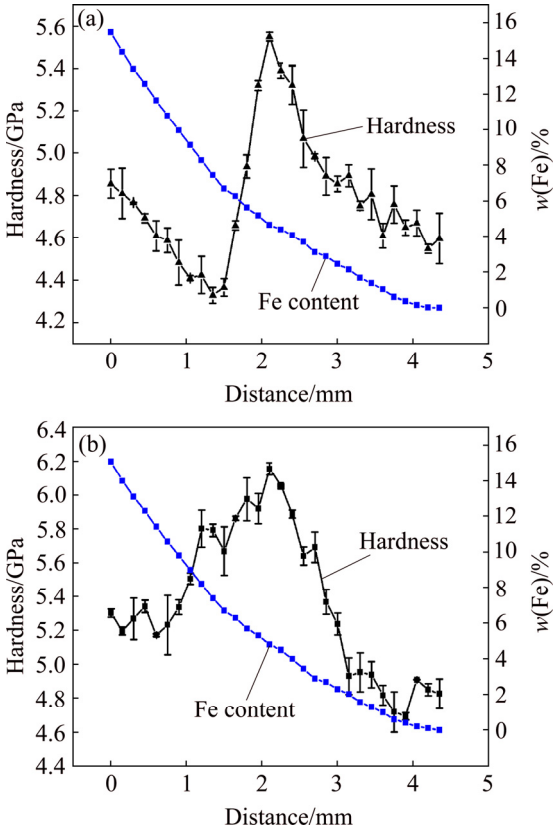

Fig. 5 Hardness and composition of series of Ti6Al4VxFe alloys: (a) After β annealing; (b) After aging

3.5 XRD results of Ti6Al4V5Fe alloy

The XRD patterns of solution-treated and as-aged Ti6Al4V5Fe alloy are shown in Fig. 6. It can be seen that after solution treatment, the sample mainly comprises α'' and β phase rather than the single β phase. No evidence of other phase (such as ω) could be seen in this stage. The new set of diffraction peaks corresponding to the hexagonal α phase after ageing at 600 °C for 6 h should be developed from α''.

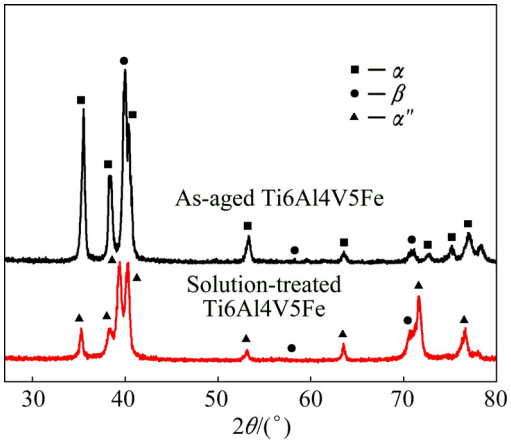

Fig. 6 XRD patterns of as-aged and solution-treated Ti6Al4V5Fe alloy

3.6 STEM results of Ti6Al4V5Fe alloy

Figure 7 displays the microstructure of Ti6Al4V5Fe upon rapid quenching from 1050 °C. The Bright field (BF) image (Fig. 7(a)) shows the nanoscale laths with two orientations which form an angle of 60° in a retained β matrix. The laths are expected to be the result of an athermal β-to-α'' transformation during quenching. These hexagonal α'' laths are too small to be detected by SEM; however, they can be clearly clarified by TEM. In Fig. 7(b), besides diffraction spots of the original β phase, extra diffraction spots are observed and identified to be orthorhombic α'' phase. The HAADF−STEM image shown in Figs. 7(c) and (d) confirms the presence of a high density of homogeneously distributed martensitic α'' laths. The average size of the laths forming in this stage is about1000 nm in length and about 50 nm in width.

The alloying element distribution in square in Fig. 7(d) is characterized by the EDS mapping (Fig. 7(e)). There is no obvious color contrast partitioning of Al, V and Fe between the α and β phases in the EDS mapping, while the line profile of Fig. 7(f) suggests that the elemental partitioning between α and β phases takes place during quenching. Solute redistribution takes place within the β phase and solute rich or lean regions form.

Microstructural features of the Ti6Al4V5Fe alloy after aging at 600 °C are shown in Fig. 8. A bright field (BF) TEM image (Fig. 8(a)) shows the homogeneously distributed, nanometer-scale, aged α precipitates within β grains. The average size of the secondary α phase is

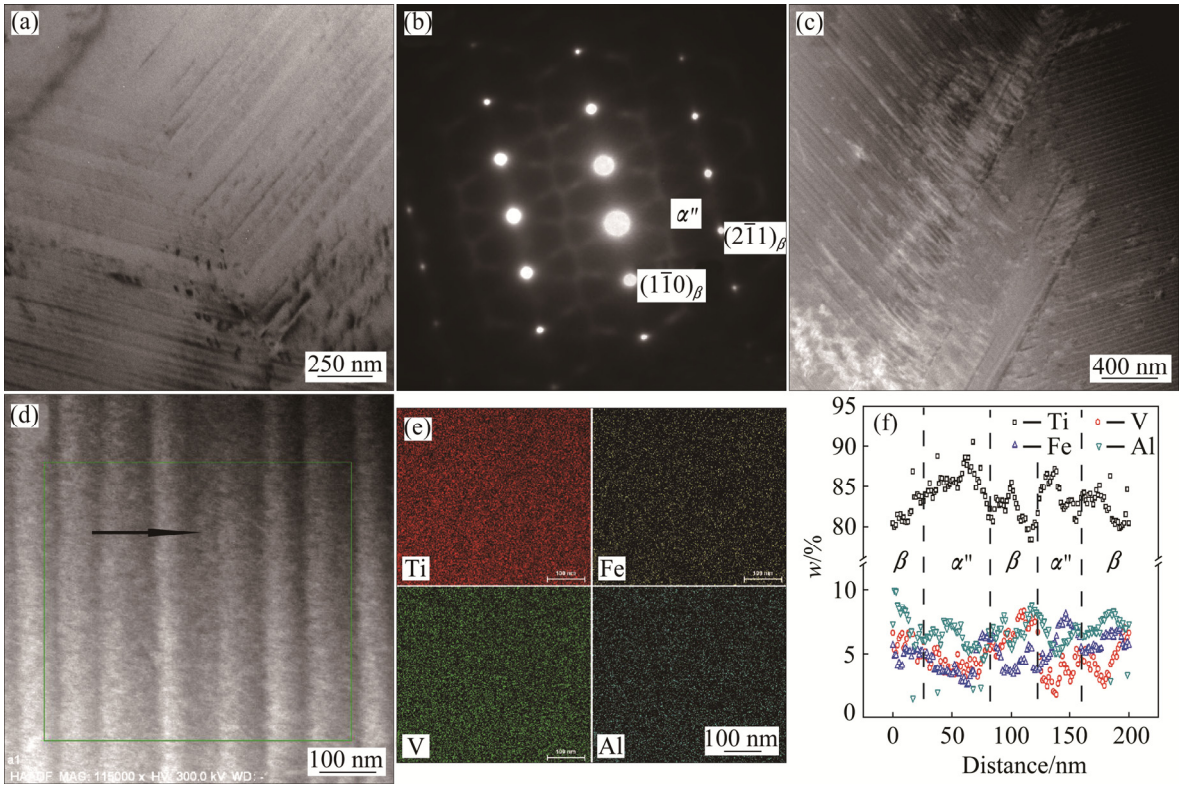

Fig. 7 Microstructural features of Ti6Al4V5Fe alloy after β annealing at 1050 °C: (a) Bright field (BF) image; (b) SAD pattern with $[113]_\beta$ zone axis; (c, d) HAADF−STEM images showing α'' laths; (e) EDS mapping of Ti, Fe, V and Al elements; (f) Composition profiles along arrows shown in (d)

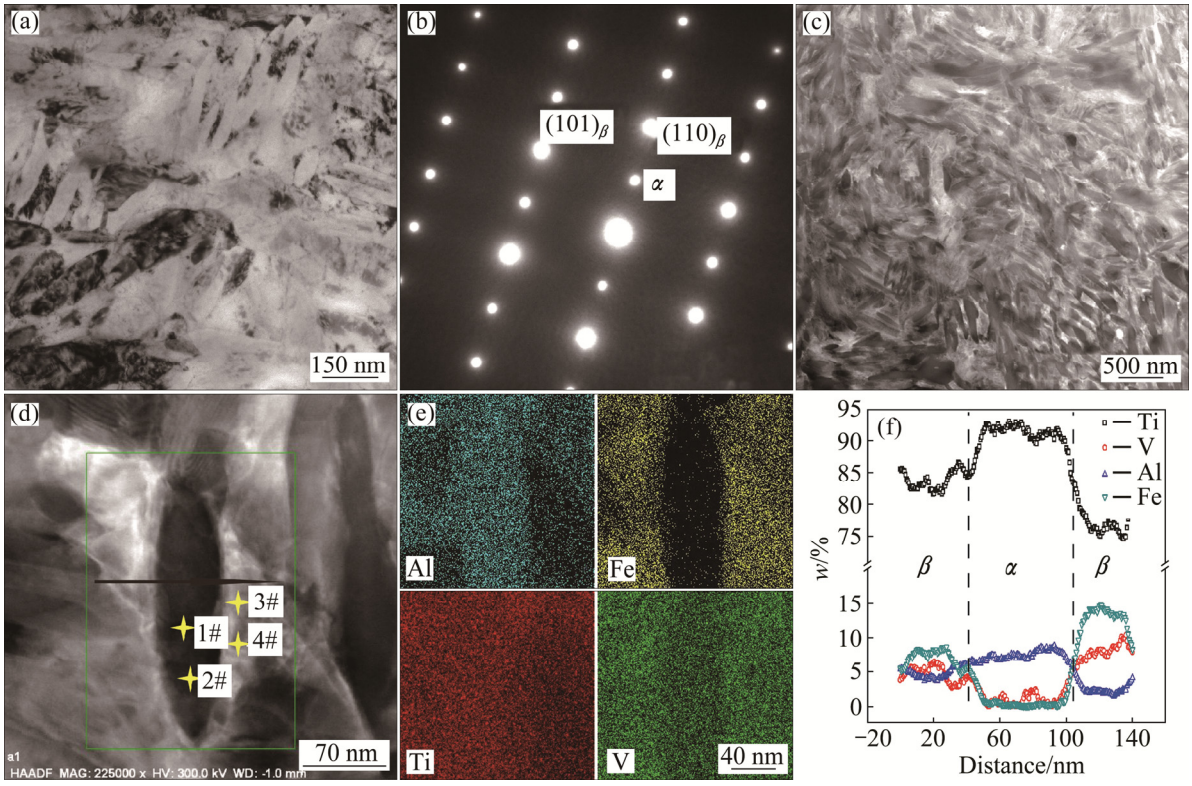

Fig. 8 Microstructural features of Ti6Al4V5Fe alloy after aging at 600 °C: (a) Bright field (BF) image; (b) SAD pattern with $[111]_\beta$ zone axis; (c, d) HAADF−STEM images showing α phase; (e) EDS mapping of Al, Fe, Ti and V elements; (f) Composition profiles along arrows shown in (d)

about 150 nm in length and about 50 nm in width. Selected-area electron diffraction patterns record along the $[111]_\beta$ zone axes are shown in Fig. 8(b), and the reflections near $1/2\{110\}_\beta$ positions arise from the α precipitates. Figure 8(c) shows a HAADF−STEM image of Ti6Al4V5Fe alloy aged at 600 °C. A content profile along the arrow in Fig. 8(d) is displayed in Fig. 8(f). The alloying element distribution in the square in Fig. 8(d) is characterized by the EDS mapping (Fig. 8(e)). The chemical compositions of the α phase and the β phase in Fig. 8(d) characterized by EDS are listed in Table 2. With ageing prolonging, the average compositions of the α and β phases become more enriched in α and β stabilizers, respectively. Al is concentrated in the α phase and while Fe and V are concentrated in the β phase.

Table 2 Chemical compositions of α and β phases in Ti6Al4V5Fe alloy after aging

Position	Phase	w(V)/%	w(Fe)/%	w(Ti)/%	w(Al)/%
1#	α	0	0.3072	92.2789	7.4137
2#	α	0	0.3044	92.4634	7.2321
3#	β	9.2843	12.2546	75.6503	2.8106
4#	β	9.3461	12.1956	76.0083	2.4498

4 Discussion

4.1 Influence of Fe content on amount and size of α phase after aging

A quantitative determination of size and volume fraction of the α phase is shown in Fig. 9. With the increase of Fe content, the volume fraction of α phase decreases with the increase of Fe content while its size first decreases and then increases. The volume fraction of α phase decreases from 89% to 3% as the Fe content increases to 15% (mass fraction). The density of α phase increases as the Fe content increases from 0 to 5%, and then decreases as the Fe content further increases. At 5% or less Fe, the martensitic starting temperature (M_s) is higher than room temperature, while the microstructures of aged α phase are significantly dependent on the quenching martensite α', as shown in Fig 3. When the alloy contains 5% or slightly more Fe, α'' or ω precipitates form within the β grains [28,29]. The nanometer-scale α'' or ω precipitates may undergo coarsening and act as heterogeneous nucleation sites for α precipitates on subsequent isothermal aging, which will produce an evenly distributed fine-scale α structure, as shown in Fig. 4(f). When 7% or more Fe is added, there are no other structural units as nucleation sites presented and the β phase is retained with bcc structure, which would lower the nucleation rate of α phase.

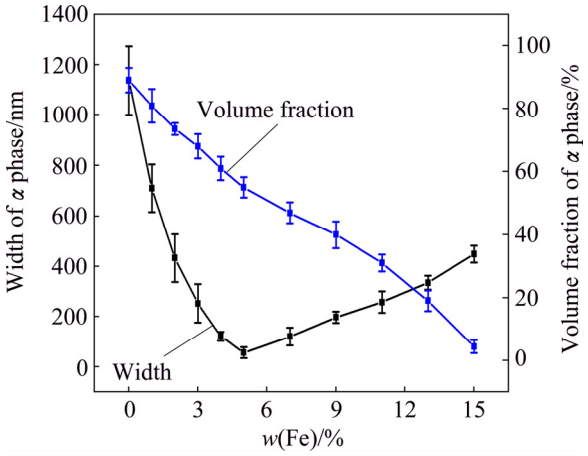

Fig. 9 Width and volume fraction of α phase as function of Fe content after aging

4.2 Phase transformation sequence of Ti6Al4V5Fe alloy

4.2.1 β-to-α'' transformation

In the β-annealed condition, a large number of nano-sized α'' phase is presented in Ti6Al4V5Fe alloy (Fig. 7). The alloying element distribution is characterized by the EDS mapping (Fig. 7(e)). There is no obvious color contrast partitioning of Al, V and Fe between the α and β phases in the EDS mapping, while the line profile of Fig. 7(f) suggests that the elemental partitioning between α and β phases takes place during quenching. Solute redistribution takes place within the β phase and solute rich or lean regions form. This does not support the theories that the α'' laths form by a shuffle mechanism without any composition difference from the β phase. The results indicate a mixed-mode β-to-α'' transformation mechanism where the displacive and diffusional components are closely coupled with each other and change concurrently, which is similar to the bainite transformation in steels [30,31]. In addition, the nanoscale α'' laths (Fig. 7(d)) may also serve as precursors/preferential nucleation sites for the formation of α phase.

4.2.2 α''-to-α transformation

In the aged condition, Ti6Al4V5Fe alloy displays the nanometer-scale acicular α precipitates, as shown in Fig. 8. The nucleation sites for the α phase within the β phase of near β titanium alloys include prior β grain boundaries, β/ω interfaces, β/β' interfaces and other defects such as dislocations and intermetallic particles within the matrix [32,33]. Depending on the overall composition of the β titanium alloy and the specific heat treatment experience of the alloy, these different sites may or may not play a substantial role in α nucleation. In the present work, there is no much dislocations in β matrix for diffusion annealing in longer time. XRD and TEM show that the sample does not contain any ω

precipitate. Typically, in Ti6Al4V5Fe alloy solution-treated above the β transus temperature and quenched, α'' lamellae form, which on subsequent isothermal aging may undergo coarsening and act as uniformly distributed heterogeneous nucleation sites for α precipitates [34]. As a consequence of such α''-assisted heterogeneous nucleation, a relatively large number of α precipitates form and uniformly distribute within the β matrix. Furthermore, these relatively fine scale α precipitates create a high number of α/β interfaces that act as dislocation barriers, and increase the strength of the alloy.

4.3 Hardness in β-annealed and aged condition

4.3.1 Hardness of Ti6Al4VxFe alloys in β-annealed condition

In the β-annealed condition, the hardness increases firstly from 4.7 to 5.6 GPa as Fe content increases from 0 to 5%, and then rapidly drops to the minimum of 4.4 GPa when the Fe content increases from 5% to 7% (mass fraction). Ti6Al4V5Fe alloy displays numerous fine lath-like α'' precipitates, and the hardness reaches the peak of 5.6 GPa, which is around 0.9 GPa higher than that of the Ti6Al4V alloy. The results demonstrate that hardness is strongly determined by the size of martensite phase. The increased hardness is mainly due to the formation of fine α'' phase during quenching. These precipitates create a high number of α''/β interfaces that act as dislocation barriers, increasing the hardness of the alloy. In addition, Fe is an effective solution strengthening element of the titanium alloys. Ti6Al4V5Fe alloy is also strengthened by the dissolved Fe atoms compared with Ti6Al4V alloy. With further increase of Fe content from 5% to 7%, the amount of α'' phase decreases, and the hardness decreases rapidly. Finally, the hardness increases slowly as the Fe content increases from 7% to 15%. This increased hardness is mainly due to the solution strengthening of Fe atoms.

4.3.2 Hardness of Ti6Al4VxFe alloys in aged condition

In the aged condition, the hardness increases firstly from 4.8 to 6.2 GPa as Fe content increases from 0 to 5% (mass fraction) and then decreases. Ti6Al4V5Fe alloy displays numerous fine lath-like α precipitates, and the hardness reaches the peak of 6.2 GPa, which is around 1.4 GPa higher than that of the Ti6Al4V alloy. Through the analysis of the microstructure, grain refinement strengthening is considered to be the main strengthening mechanism. The hardness is strongly determined by the size of α phase. Compared with Ti6Al4V, the α size of Ti6Al4V5Fe is about 0.1 μm and the grain boundary/phase boundary increases, which leads to the huge blocking effect on dislocation slippage. In addition, the α precipitate is the harder phase and the β phase is the softer phase. The fine α phase can hinder the movement of the dislocations and thus strengthen the alloys [35].

It should be noted that the volume fraction of α phase is another important factor which has significant influence on the properties of titanium alloys. It is found that high strength can be got in the near β titanium alloys with fine scale as well as the optimal (52%−60%) volume fraction of α phase [10,36,37]. Ti6Al4V5Fe has small size and reasonable (about 55%) volume fraction of α phase, which could be another reason for the peak hardness.

KANOU et al [19] have investigated the effect of Fe addition on the mechanical properties of Ti6Al4V alloys. The results show that the tensile strength of the Ti6Al4V4Fe alloys is 30% greater than that of the Fe-free alloys. ABBASI et al [18] have verified the excellent hot working performance of Ti6Al6Mo6Fe3Al alloy. Considering the results of this and previous work, Ti6Al4V5Fe alloy will be more promising as a high-strength titanium alloy.

5 Conclusions

1) With the increase of Fe content to 5% (mass fraction), the amount of α' phase after quenching decreases to zero, the amount of equilibrium α phase after aging decreases to about 55%, the size of α phase decreases to sub-micron level, and the hardness after quenching and aging increases and reaches the peak value. Further increase of Fe content increases the size of α phase and decreases the hardness after aging.

2) The highest hardness after quenching may be due to the formation of fine α'' phases, which subsequently acts as uniformly distributed heterogeneous nucleation sites for α precipitates during aging and leads to the peak hardness after aging.

References

[1] BANERJEE D, WILLIAMS J C. Perspectives on titanium science and technology [J]. Acta Materialia, 2013, 61: 844−879.

[2] DURAISELVAM M, VALARMATHI A, SHARIFF S M, PADMANABHAM G. Laser surface nitrided Ti−6Al−4V for light weight automobile disk brake rotor application [J]. Wear, 2014, 309: 269−274.

[3] FAN Xiao-guang, YANG He, GAO Peng-fei, ZUO Rui, LEI Peng-hui, JI Zhe. Morphology transformation of primary strip α phase in hot working of two-phase titanium alloy [J]. Transactions of Nonferrous Metals Society of China, 2017, 27: 1294−1305.

[4] BENEA L, DANAILA E, PONTHIAUX P. Effect of titania anodic formation and hydroxyapatite electrodeposition on electrochemical behaviour of Ti−6Al−4V alloy under fretting conditions for biomedical applications [J]. Corrosion Science, 2015, 91: 262−271.

[5] ZHANG Ling-bo, WANG Ke-zheng, XU Li-juan, XIAO Shu-long, CHEN Yu-yong. Effect of Nb addition on microstructure, mechanical properties and castability of β-type Ti−Mo alloys [J]. Transactions of Nonferrous Metals Society of China, 2015, 25: 2214−2220.

[6] ZHANG Shou-yin, LI Jin-shan, KOU Hong-chao, YANG Jie-ren, YANG Guang, WANG Jun. Microstructure evolution of isothermal holding treatment during melt solidification of Ti−6Al−4V alloy [J]. Transactions of Nonferrous Metals Society of China, 2015, 25: 1091−1096.

[7] BALASUBRAMANIAN M. Development of processing windows for diffusion bonding of Ti−6Al−4V titanium alloy and 304 stainless steel with silver as intermediate layer [J]. Transactions of Nonferrous Metals Society of China, 2015, 25: 2932−2938.

[8] RAGHUNATHAN S L, DASHWOOD R J, JACKSON M, VOGEL S C, DYE D. The evolution of microtexture and macrotexture during sub-transus forging of Ti−10V−2Fe−3Al [J]. Materials Science and Engineering A, 2008, 488: 8−15.

[9] SANTHOSH R, GEETHA M, SAXENA V K, NAGESWARARAO M. Studies on single and duplex aging of metastable beta titanium alloy Ti−15V−3Cr−3Al−3Sn [J]. Journal of Alloys and Compounds, 2014, 605: 222−229.

[10] JONES N G, DASHWOOD R J, JACKSON M, DYE D. β Phase decomposition in Ti−5Al−5Mo−5V−3Cr [J]. Acta Materialia, 2009, 57: 3830−3839.

[11] HSU H C, HSU S K, WU S C, LEE C J, HO W F. Structure and mechanical properties of as-cast Ti−5Nb−*x*Fe alloys [J]. Materials Characterization, 2001, 61: 851−858.

[12] HUANG S X, ZHANG X D, JIANG Y, JIANG Y R, MAO C, WU D, ZHANG L G, LIU L B. Experimental investigation of Ti−Nb−Co ternary system at 1000 °C [J]. Materials and Design, 2017 115: 170−178.

[13] WANG C S, ZHANG K S, PANG H J, CHEN Y Z, DONG C. Laser-induced self-propagating reaction synthesis of Ti−Fe alloys [J]. Journal of Alloys and Compounds, 2008, 43: 218−221.

[14] LIN D J, LIN J H C, JU C P. Structure and properties of Ti−7.5Mo−*x*Fe alloys [J]. Biomaterials, 2002, 23: 1723−1730.

[15] LOUZGUINE D V, KATO H, INOUE A. High strength and ductile binary Ti−Fe composite alloy [J] Journal of Alloys and Compounds, 2004, 384: L1−L3.

[16] SRINIVASU G, NATRAJ Y, BHATTACHARJEE A, NANDY T K, NAGESWARA RAO G V S. Tensile and fracture toughness of high strength β Titanium alloy, Ti−10V−2Fe−3Al, as a function of rolling and solution treatment temperatures [J]. Materials and Design, 2013, 47: 323−330.

[17] WEISS I, SRINIVASAN R, SAQIB M, STEFANSSON N, JACKSON A G, LECLAIR S R. Bulk deformation of Ti−6.8Mo−4.5Fe−1.5Al (trimetal LCB) alloy [J]. Journal of Materials Engineering and Performance, 1996, 5: 335−352.

[18] ABBASI S M, MOMENI A, AKHONDZADEH A, GHAZI MIRSAED S M. Microstructure and mechanical behavior of hot compressed Ti−6V−6Mo−6Fe−3Al [J]. Materials Science and Engineering A, 2015, 639: 21−28.

[19] KANOU O, FUKADA N, HAYAKAWA M. The effect of Fe addition on the mechanical properties of Ti−6Al−4V alloys produced by the prealloyed powder method [J]. Materials Transactions, 2016, 57: 681−685.

[20] SAMAL S, AGARWAL S, GAUTAM P, BISWAS K. Microstructural evolution in novel suction cast multicomponent Ti−Fe−Co alloys [J]. Metallurgical and Materials Transactions A, 2015, 46: 851−868.

[21] SHI X Z, MA S Y, LIU C M, WU Q R, LU J P, LIU Y D, SHI W T. Selective laser melting-wire arc additive manufacturing hybrid fabrication of Ti−6Al−4V alloy: Microstructure and mechanical properties [J]. Materials Science and Engineering A, 2017, 684: 196−204.

[22] ZHAO J C, ZHENG X, CAHILL D G. High-throughput diffusion multiples [J]. Materials Today, 2005, 12: 28−37.

[23] ZHAO J C. The diffusion-multiple approach to designing Alloys [J]. Annual Review of Materials Research, 2005, 35: 51−73.

[24] WU D, ZHANG L G, LIU L B, SHI X, HUANG S X, JIANG Y. Investigation of the influence of Fe on the microstructure and properties of Ti5553 near-β titanium alloy with combinatorial approach [J]. International Journal of Materials Research, 2017, 108: 355−363.

[25] ZHANG X D, LIU L B, ZHAO J C, WANG J L, ZHENG F, JIN Z P. High-efficiency combinatorial approach as an effective tool for accelerating metallic biomaterials research and discovery [J]. Materials Science and Engineering C, 2014, 39: 273−280.

[26] HSU H C, WU S C, HSU S K, CHEN C Y, HO W F. Machinability evaluation of Ti−5Nb−*x*Fe alloys for dental applications [J]. Materials Science and Engineering A, 2014, 606: 157−164.

[27] HO W F, PAN C H, S C WU, HSU H C. Mechanical properties and deformation behavior of Ti−5Cr−*x*Fe alloys [J]. Journal of Alloys and Compounds, 2009, 472: 546−550.

[28] YAO T T, DU K, HAO Y L, LI S J, YANG R, YE H Q. In-situ observation of deformation induced α'' phase transformation in a β-titanium alloy [J]. Materials Letters, 2016, 182: 281−284.

[29] SONG M, HE S Y, DU K, HUANG Z Y, YAO T T, HAO Y L, LI S J, YANG R, YE H Q. Transformation induced crack deflection in a metastable titanium alloy and implications on transformation toughening [J]. Acta Materialia, 2016, 118: 120−128.

[30] DEVARAJ A, NAG S, SRINIVASAN R, WILLIAMS R E A, BANERJEE S, BANERJEE R, FRASER H L. Experimental evidence of concurrent compositional and structural instabilities leading to ω precipitation in titanium–molybdenum alloys [J]. Acta Materialia, 2012, 60: 596−609.

[31] NAG S, ZHENG Y, WILLIAMS R E A, DEVARAJ A, BOYNE A, WANG Y, COLLINS P C, VISWANATHAN G B, TILEY J S, MUDDLE B C, BANERJEE R, FRASER H L. Non-classical homogeneous precipitation mediated by compositional fluctuations in titanium alloys [J]. Acta Materialia, 2012, 60: 6247−6256.

[32] AHMED M, LI T, CASILLAS G, CAIRNEY J M, WEXLER D, PERELOMA E V. The evolution of microstructure and mechanical properties of Ti−5Al−5Mo−5V−2Cr−1Fe during ageing [J]. Journal of Alloys and Compounds, 2015, 629: 260−273.

[33] NAG S, BANERJEE R, SRINIVASAN R, HWANG J Y, HARPER M, FRASER H L. ω-Assisted nucleation and growth of α precipitates in the Ti−5Al−5Mo−5V−3Cr−0.5Fe β titanium alloy [J]. Acta Materialia, 2009, 57: 2136−2147.

[34] OHMORI Y, OGO T, NAKAI K, KOBAYASHI S. Effects of ω-phase precipitation on $\beta\rightarrow\alpha$, α'' transformations in a metastable β titanium alloy [J]. Materials Science and Engineering A, 2001, 312: 182−188.

[35] NYAKANA S L, FANNING J C, BOYER R R. Quick reference guide for β titanium alloys in the 00s [J]. Journal of Materials Engineering and Performance, 2005, 14: 799−811.

[36] WAIN N, HAO X J, RAVI G A, WU X. The influence of carbon on precipitation of α in Ti−5Al−5Mo−5V−3Cr [J]. Materials Science and Engineering A, 2010, 527: 7673−7683.

[37] KAR S K, GHOSH A, FULZELE N, BHATTACHARJEE A. Quantitative microstructural characterization of a near beta Ti alloy, Ti-5553 under different processing conditions [J]. Materials Characterization, 2013, 81: 37−48.

扩散偶法研究 Fe 含量对 Ti6Al4V 组织和性能的影响

吴 迪[1]，章立钢[1,2]，刘立斌[1,3]，白伟民[1]，曾丽君[1]

1. 中南大学 材料科学与工程学院，长沙 410083；
2. ZIK Virtuhcon, TU Bergakademie Freiberg, Fuchsmühlenweg 9, D-09596 Freiberg, Germany;
3. 中南大学 有色金属材料科学与工程教育部重点实验室，长沙 410083

摘　要：采用扩散偶实验方法研究 Fe 含量对 Ti6Al4V 合金显微组织和性能的影响。通过制作 Ti6Al4V−Ti6Al4V20Fe 扩散偶，在 1000 ℃ 经 600 h 扩散退火，在一个样品内获得具有连续成分梯度的合金。结合电子探针、扫描电镜和纳米压痕，确定 Ti6Al4V*x*Fe 合金成分−组织−硬度的关系。当合金中 Fe 含量增加到 5%(质量分数)时，时效状态下合金中的 α 相体积分数降低到 55%，同时合金具有最高的硬度，Ti6Al4V5Fe 合金将是 Ti6Al4V*x*Fe 体系中最具前景的合金。HAADF−STEM 和 XRD 结果表明，Ti6Al4V5Fe 合金在固溶淬火阶段生成纳米尺寸 α'' 层片，这些亚稳的 α''层片在随后的时效过程中逐渐长大，并作为 α 相的形核核心，形成稳定 α 相。

关键词：扩散偶；Ti6Al4V*x*Fe 合金；成分；组织；硬度；HAADF−STEM

(Edited by Bing YANG)